Title
CONTINUOUS ANNEALING OF A Fe/0.1C/0.45Si/ 0.05Nb/0.1Mo DUAL PHASE STEEL

Authors
Gau, J.S.
Thomas, G.

Publication Date
1983-04-01

Lawrence Berkeley Laboratory
UNIVERSITY OF CALIFORNIA

Materials & Molecular
Research Division

Presented at the 111th Annual Meeting of the American Institute of Mining, Metallurgical and Petroleum Engineers, Dallas, TX, February 14-18, 1982; and to be published in the Proceedings

CONTINUOUS ANNEALING OF A Fe/0.1C/0.45Si/0.05Nb/0.1Mo DUAL PHASE STEEL

J.S. Gau and G. Thomas

April 1983

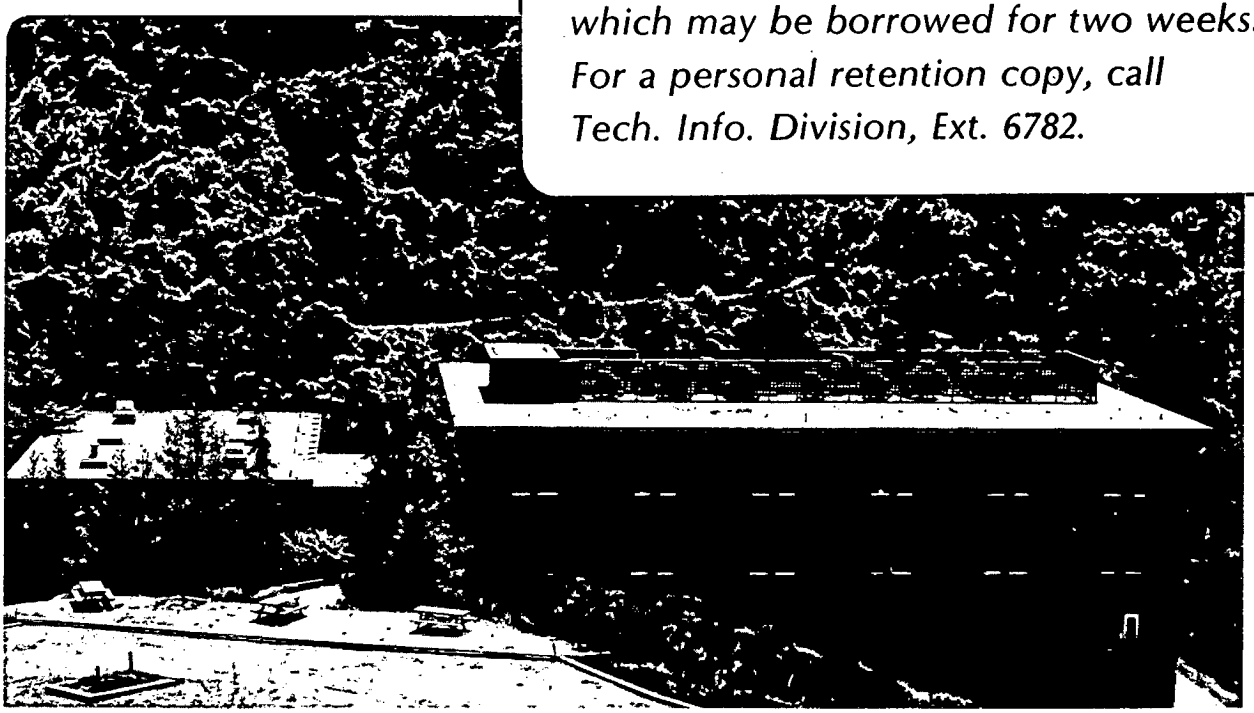

Prepared for the U.S. Department of Energy under Contract DE-AC03-76SF00098

DISCLAIMER

Continuous Annealing of a Fe/0.1C/0.45Si/0.05Nb/0.1Mo Dual Phase Steel

J. S. Gau and G. Thomas

Materials and Molecular Research Division,
Lawrence Berkeley Laboratory,
University of California,
Materials Science and Mineral Engineering Department,
University of California, Berkeley, CA 94720

ABSTRACT

Several two phase annealing heat treatments have been performed on a Nb and Mo microalloyed low carbon steel. Continuous intercritical annealing followed by water quenching produces a coarse ferrite-martensite structure that has the highest tensile strength of all heat treatments utilized. The high strength arises from a combination of the dispersion hardening which occurs in ferrite and the presence of martensite. It is concluded that the ferrite forming elements Nb and Mo do not benefit hardenability in this steel for dual phase heat treatment, in thicknesses ~5mm.

INTRODUCTION

Considerable interest in the development of low carbon dual phase steels has been well documented[1-4] and has provoked extensive research activity. During the past decade, great effort has been extended to demonstrate that various industrial processes (e.g. Table 1) can be used to produce duplex ferritic and martensitic (DFM) microstructures from plain carbon steels usually containing microalloying additions e.g. V, Nb etc. Previous research has been directed toward obtaining "clean" ferrites by choosing appropriate austenite-forming elements[5] to improve the formability of high strength low alloy (HSLA) steels to meet the needs

of the automobile industry. This results in a decrease in the amount of dissolved carbon in the ferrite by enhancing the partitioning of carbon between austenite and ferrite during intercritical annealing. However, the existence of precipitates in the ferrite matrix, even with austenite-forming additions, has only very recently been reported and characterized[3,6]. With the implication of precipitation strengthening, it is interesting to exploit further the potential applications of low carbon steels containing carbide-forming elements. They form a new class of dual phase steels characterized by precipitation in the ferrite matrix.

For a given composition, the mechanical properties of dual phase steels are mainly governed by the composite morphology[7], volume fraction of martensite, and other phases e.g. retained austenite and precipitates in the ferrite matrix etc. All these are functions of process variables such as the annealing temperature, cooling rate following the intercritical annealing and the transformation path. From a steel production viewpoint, it is essential to optimize the microstructure, and hence properties, economically through the control of process techniques.

The main objective of the present work, then is to examine and understand the structure-property-process relationship of a low carbon steel, Fe/0.45Si/0.05Nb/0.1Mo/0.1C. Using transmission electron microscopy (TEM) it is possible to monitor the changes in microstructure produced by the process variables, cooling rates and transformation path, and to characterize the precipitates formed and the role they play in the strengthening behavior. The microstructure and tensile properties can then be correlated.

EXPERIMENTAL PROCEDURES

A. Material Preparation

The Fe/C/Si system[8] which has been well characterized has been selected

as the base alloy. The composition of the experimental alloy, which was provided by Climax Molybdenum Corporation is as follows (wt percent)

Fe	C	Si	Nb	Mo
Balance	0.1	0.45	0.05	0.1

The as-received material was first homogenized in argon at 1100°C for 24 hours, forged and then rolled into a plate of 3/8" x 3" cross section. Slightly oversized tensile blanks were cut with the tensile axis parallel to the rolling direction.

B. Heat Treatment and Tensile Testing

The different dual phase heat treatment processes are plotted in the schematic diagram of Figure 1. Various cooling rates after intercritically annealing were carried out ranging from ice-brine quenching (1000°C/sec) to air cooling (3°C/sec). These rates were measured by a chromel-alumel thermocouple at the center of each specimen.

C. Metallography and X-ray Analysis

Optical metallography was used to examine the morphology of specimens etched in 2% Nital.

Foils for transmission electron microscopy (TEM) were made by twin-jet polishing with a chromic and acetic solution and examined in a Philips EM 301 microscope and also in an analytical Philips EM 400 microscope. The latter was used to identify the inclusions and in an attempt to study the partitioning of microalloying elements.

The X-ray method developed by Miller[9] was utilized to determined the volume fraction of retained austenite in the dual phase structures obtained. The G.E. Drano X-ray diffractometer with filtered Mo Kα radiation was used to analyse the specimens. The results showed that no austenite could be

detected by this method. The TEM results also agree with this result so the % austenite, if present, must be less than 1%.

RESULTS

A. Metallography and Microstructure

1. Effect of Cooling Rate. All air cooling and forced air cooling processes either from single phase or two phase regions resulted in a microstructure comprised mainly of relatively clean ferrite and pearlite with an average interlamellar spacing of 0.05μ. A typical microstructure of degenerate pearlite[10] was also observed, when the cooling rate was fast enough (i.e. an oil quench) to ensure the formation of martensite after intercritical annealing.

2. Effect of Transformation Path

(a) Optical Metallography - Figures 3(a), (b), and (c), illustrate the resultant duplex phase structure formed following different transformation paths. For the direct intercritical annealing (Process I), the dominant nucleations sites of the γ phase during the annealing are ferrite-cementite boundaries, and ferrite grain boundaries. This produces fine globular martensite dispersed in a ferrite matrix with a grain size of $\sim$20 microns. In the continuous intercritical annealing (Process II), the ferrite nucleates and grows from the unstable austenite during the annealing. The resultant coarse two phase morphology indicates that this heat treatment scheme has no grain refinement effect. Finally, for the case of the intermediate intercritical annealing (Process III), reheating to the two phase annealing temperature from the initial $\sim$100% martensite involves the nucleation of ferrite at prior austenite grain boundaries, martensite lath boundaries and possibly other lattice defects.

The martensite decomposes to ferrite during reheating, analogous to the decomposition of martensite during tempering. The resultant fibrous morphology indicates the austenite formed during the annealing grows in an acicular manner along martensite lath boundaries.

(b) TEM Observations - Extensive electron microscopy studies have been performed to characterize the resultant DFM structures. A summary of the microstructure characterization is presented in TABLE II.

The low carbon dual phase steel consists mainly of dislocated martensite with some microtwins as shown in Figure 4. It has been known[11] that during the intercritical annealing, equilibrium partition of the substitutional elements is not achieved. It is likely that carbon is also not completely partitioned though it diffuses an order of magnitude faster than the substitutional elements. Consequently, a high concentration can exist even within a single austenite grain. This accounts for the occurrence of microtwins as observed.

The ferrite matrix contains extensive precipitation. Figure 5 shows the fine plate-like precipitates randomly dispersed in the ferrite matrix. With the beam parallel to the [001] zone axis, the edge-on precipitates reveal two out of three variants of platelet precipitates because of the contrast conditions (g·b factor) see reference 6. Careful tilting experiments and trace analysis show that in the dual phase heat treatments the strong carbide forming elements produce plate precipitates of 10nm mean diameter oriented on or within 10° of {100} ferrite habit planes. The precipitation reaction in this study exhibits the general features of grain boundary precipitates-free zones and dislocations free from precipitates[12] as can be seen in Figure 6. It is noted that in addition to the matrix precipitation due to quenching, interphase precipitation[13]

of niobium carbides is observed after Processes I and II. The banded dispersed precipitation (Figure 7) accompanies the moving $\gamma \rightarrow \alpha$ interphase boundary during the $\gamma \rightarrow \alpha$+carbide isothermal decomposition. This interphase precipitation[13] is known to be a common precipitation mode for alloy carbonitrides in microalloyed steels containing carbide-forming elements, such as V[14], Nb[10], Mo etc. This phenomenon offers a new systematic approach to alloy design by providing the direct route of precipitation hardening in contrast to the conventional quenching and aging process. A quantitative result will be presented in a latter section to illustrate the correlation between precipitate morphology between precipitate morphology and tensile strength.

It is not intended in this study to characterize the precipitation process. Fundamental studies regarding the precipitation mechanisms have been carried out recently[6,15].

B. Mechanical Properties

The mechanical property data in this investigation are summarized in Table III.

The variation of strength as a function of cooling rate using Process II is plotted in Figure 8. It can be seen that ultimate tensile strength, yield strength and the U.T.S./Y.S. ratio increase with cooling rate up to 1000°/sec. The characteristics of the dual phase steel, i.e., high work hardening rate, high U.T.S./Y.S. ratio and continuous yielding are attributed to the formation of martensite as the load-carrying constituent dispersed in the ferrite matrix.

The role of composite morphology due to the transformation path is reflected in the mechanical properties. The morphology and property results

are similar to those reported for a Fe/2.0Si/0.1C dual phase steel[7]. The coarse two phase morphology (Figure 3(b)) yields the highest strength among all dual phase heat treatments tried. The high strength is due to the large size of martensite islands and to the significant precipitation present in the ferrite. However, the poor ductility is also due to the precipitation and the large ferrite grain size, due to the dislocation interactions with the substructure such as precipitates, inclusions, etc. Recently, an in-situ electron microscopy deformation experiment[16] has clearly demonstrated that ductile fracture occurs with cracks initiating within the interior of ferrite, confirming the fracture analysis[7] of dual phase steels. The fibrous morphology produced in the Process III has the best ductility. This morphology is most efficient in load transfer. The transfer of load occurs by shear action along the particle/matrix interface. For a given volume fraction of second phase, since more interfacial area is available in the case of a fibrous morphology, a better ductility is therefore established, due to the efficiency of stress transfer across the interface.

The presence of carbide forming elements Nb and Mo, produces extensive precipitation in ferrite. Here, a quantitative result is presented to illustrate the strengthening due to precipitation for a given martensite volume fraction (0.4). According to the Ashby-Orowan model[17] of precipitation strengthening, the resolved shear stress ζ overcome the obstacles of moving dislocations can be expressed as:

$$\zeta(\text{MPa}) = \frac{1}{1.18} \frac{1.2Gb}{2\pi L} \ln\left(\frac{\bar{X}}{2b}\right) \qquad \text{(A)}$$

where G is the shear modulus which is 80,300 MPa for ferrite, b is the magnitude of the dislocation Burgers vector (2.5Å for ferrite), L is the

free spacing between particles and $\overline{X}$ is the mean effective particle diameter. Assuming that the tensile stress $\sigma \approx 2\zeta$, equation (A) can be rewritten as:

$$\sigma = 0.33 \frac{Gb}{L} \ln \left(\frac{\overline{X}}{2b}\right)$$

In the continuous intercritical annealing, L is taken as the average spacing between interphase precipitation bands, i.e., $L = (1.6 \pm 0.1) \times 10^{-2}$; $\overline{X}$ is determined by examining the average spheroidal particle diameter $\overline{D}$ of precipitates in the dark field EM images, following the Fullman equation[18].

$$\overline{X} = \overline{D} \left(\frac{2}{3}\right)^{1/2} = (33 \pm 8)\ \text{Å}$$

This approximation yields the tensile strength 780 ± 40 MPa in agreement with experimental data. The implication of this approximation with respect to higher strength is obvious. The strength is governed by the size of precipitates and spacing between the bands in the interphase structure. Intercritical annealing temperature is therefore another important process factor which will affect these parameters.

DISCUSSION

The present results indicate that the microalloying elements Nb and Mo do not significantly benefit the hardenability in the two phase treatments (Figure 8). Fast quenching ($\geq$ 80°C/sec) after intercritical annealing is necessary to accomplish martensite formation. Although X-ray microanalysis has failed to resolve the partitioning of microalloying elements during STEM studies, significant precipitates in the ferrite matrix and the absence of retained austenite support the fact that carbon atoms do not partition to the unstable austenite during the

intercritical annealing.

It is noted that the precipitation process is a complicated one. Alternative modes of alloy carbide precipitation can occur when precipitates nucleate in austenite before or in the supersaturated ferrite following the motions of the γ/α interface during isothermal decomposition. It is impossible to measure each parameter quantitatively by examining the specimens at room temperatures. Special attention and techniques such as resistivity measurements as a function of temperature and time are needed. Qualitatively, all the transformation behavior starting with 100% austenite can be understood with the aid of a precipitation-recrystallization-temperature-time (PRTT) diagram[19] in addition to the continuous cooling-temperature-time (CCT) diagram[20]. A schematic representation utilizing these ideas is shown in Figure 9. This combined diagram represents a model which could be adapted to facilitate practical control of processing and serve as a basis for understanding the process-structure-property relations for continuous annealing conditions. It should be noted of course, that this diagram is not applicable to Process I and III neither of which starts with austenite.

The continuous intercritical annealing process used in this investigation produces no ferritic grain refinement effect and consequently the alloys has poor ductility. Strength, ductility and toughness are the most important properties for structural steels. Only through the control of the grain size can all these parameters be optimized. The carbide forming elements are known to retard austenite recrystallization[19] through either a "solute drag" or a "precipitation pinning" effect. It is therefore possible to refine the final ferritic grain size by controlled rolling

so as to enhance carbides precipitation in the austenite region as indicated in the PRCC diagram. This is similar to the ausforming process to produce carbides in austenite[21].

To summarize, the characteristics of the natural composite dual phase steels have been understood qualitatively through the structure-property relationships. The continuous process (Process II) is designed to simulate hot-rolling as done industrially. The advantages of this process viz. in simplicity and energy saving are obvious. Further work along the lines suggested here should be promising.

CONCLUSION

1. The microalloying elements Nb and Mo are not effective for hardenability in the base Fe/0.45Si/0.1C steel. A fast quenching rate (cooling rate after intercritical annealing ($\geq$80°C/sec) is required to obtain a duplex ferritic-martensitic microstructure).

2. In addition to fine platelet precipitates in the ferrite matrix, interphase precipitation of niobium carbides is observed after Process I and II, but not from Process III. The Ashby-Orowan model of precipitation strengthening successfully predicts the tensile strength found for the continuous intercritical annealing process (Process II).

3. Better ductility can be achieved when a fibrous morphology is obtained. On the other hand, higher strength is obtained with a coarse dual phase morphology.

4. Continuous annealing together with controlled rolling of dual phase steels is very promising both from an economic and practical viewpoint.

ACKNOWLEDGEMENTS

The authors would like to thank Climax Molybdenum Company for kindly supplying the material.

Thanks are also extended to Drs. R. Hoel, J.J. Rayment and J.Y. Koo for their comments and assistance. This work is supported by the Director, Office of Energy Research, Office of Basic Energy Sciences, Materials Science Divisin of the U.S. Department of Energy under Contract No. DE-AC03-76SF00098.

TABLE 1

Processes Available to Produce Dual-Phase Low Carbon Steels

1. As hot-rolled condition
2. Intercritically annealed condition
3. Gamma phase annealed condition
4. Batch-annealed condition
5. Continuous annealing and processing condition

TABLE II

Process Path Effect on Final Microstructure

Heat Treatment	Morphology of Martensite	Precipitate density in ferrite
I. Direct Annealing	Globular	$(3\pm1) \times 10^{16}/cm^3$
II. Continuous Annealing	Coarse	$(5\pm1) \times 10^{16}/cm^3$
III. Intermediate Annealing	Fibrous	$\sim 10^{15}/cm^3$

TABLE III

Process Path Effect on the Tensile Properties

Heat Treatment	U.T.S. KSI	U.T.S. MPa	Y.S. KSI	Y.S. MPa	E_t (%)	E_u (%)	Y.S./U.T.S.
1. Direct Annealing	106	730	70	482	15	11	0.66
2. Continuous Annealing	115	790	75	517	13	9	0.65
3. Intermediate Intercritical Annealing	105	724	81	558	20	15	0.77

REFERENCES

1. Production and Properties of Vanadium Dual Phase Steel and Cold Pressing Steels in the Automobile Industry, Proceedings of a Seminar in Berlin, Vanadium International Technical Committee, October 1978.
2. Formable HSLA and Dual-Phase Steels, A.T. Davenport, ed., AIME, Warrendale, PA (1979).
3. Structure and Properties of Dual Phase Steel, R. A. Kot and J.W. Morris, eds., AIME, New York, N.Y. (1979).
4. Fundamentals of Dual Phase Steel, R.A. Kot and B. L. Brainfitt, eds., AIME, New York (1981), in press.
5. T. Furukawa, H. Morikawa, H. Takechi and K. Koyama, in Structure and Properties of Dual Phase Steels, p. 281, AIME, New York (1979).
6. R. Hoel and G. Thomas, Scripta Met., 1981, Vol. 15, p. 867.
7. N.J. Kim and G. Thomas: Met. Trans. 1981, Vol. 12A, p. 483.
8. J.Y. Koo and G. Thomas: Met. Trans. 1977, Vol. 8A, p. 525; Met. Trans. 1980, Vol. 11A, p. 852.
9. R. L. Miller, Trans. A. S. M. 1964, Vol. 57, p. 892.
10. M. Geib, D.K. Matlock and G. Krauss: Met. Trans. 1980, Vol. 11A, p. 1683.
11. W. S. Owen: Met. Tech. 1980, Vol. 7, p. 1.
12. J.S. Gau, J.Y. Koo, A. Nakagawa and G. Thomas, to be published in Fundamentals of Dual Phase Steels (1981), in press.
13. R.W.K. Honeycombe: Met. Trans. 1976, Vol. 7A, p. 915.
14. A. Nakagawa, J.Y. Koo and G. Thomas: Met. Trans. 1981, Vol. 12A, p. 1965.

15. A.R. Pelton and K.H. Westmacott, to be published in the International Conference on Solid-Solid Phase Transformations, Pittsburgh, PA, 1981.

16. G. Thomas, (unpublished research).

17. T. Gladman, D. Dulieu and I.D. McIvor, in Microalloyings 75, p. 32, Proceedings, Union Carbide Company, Washington D.C. (1977).

18. R.L. Fullman: Trans. A.I.M.E., 1953, Vol. 197, p. 447.

19. S.S. Hansen: J.B. VanderSande and M. Cohen: Met. Trans., 1980, Vol. 11A, p. 387.

20. A. P. Goldren and G.T. Eldis: J. Metals, 1980, Vol. 32, p. 41.

21. O. Johari and G. Thomas, A.S.M. Trans., 1965, Vol. 58, p. 563.

FIGURE CAPTIONS

Fig. 1. Schematic representation of the dual phase heat treatment processes.

Fig. 2. Transmission electron micrographs showing (a) pearlite, (b) ferrite in the forced air cooling specimen (Process I).

Fig. 3. Optical micrographs of the duplex ferritic-martensitic microstructure developed in each heat treatment process as indicated.

Fig. 4. Transmission electron micrographs showing typical microtwins observed in martensite phase in the dual phase steels (a) bright field, (b) dark field (Process III).

Fig. 5. Transmission electron micrographs showing precipitates in ferrite phase: (a) plate-like precipitates with electron beam parallel to [001] axis, (b) tilting away from [001] shows contrast typical of vacancy type particles surrounded by dislocation loops (Process II).

Fig. 6. Transmission electron micrographs (a) bright field, (b) dark field, showing the precipitates and extinction fringes observed in the ferrite phase following heat treatment Process I.

Fig. 7. Transmission electron micrograph showing interphase precipitation in the ferrite matrix, observed after Process I and II but not III.

Fig. 8. Plot of the field and tensile strengths as a function of cooling rate, (Process I and II).

Fig. 9. Schematic sketch illustrating the model proposed for the precipitation-recrystallization-continuous cooling-temperature-time diagram and, the corresponding microstructure developed at each step (a-d) as indicated.

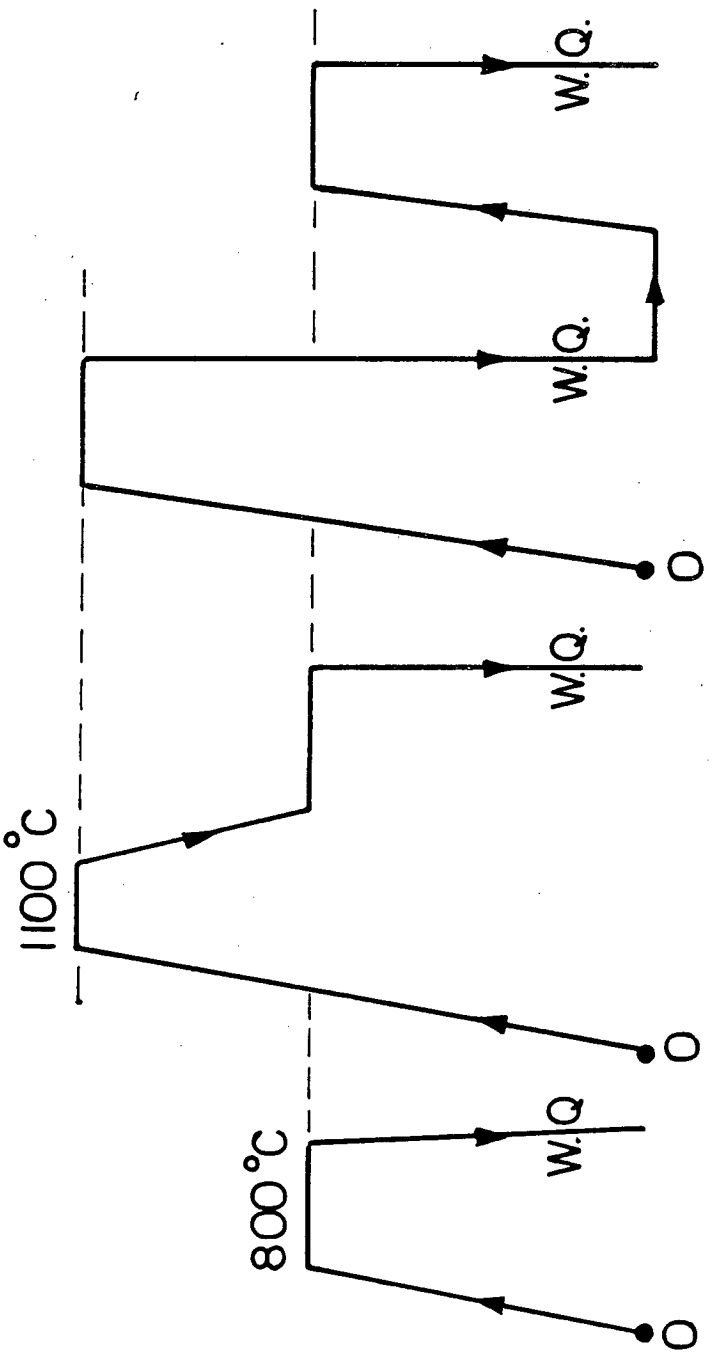

XBL8010-6189

Fig. 1

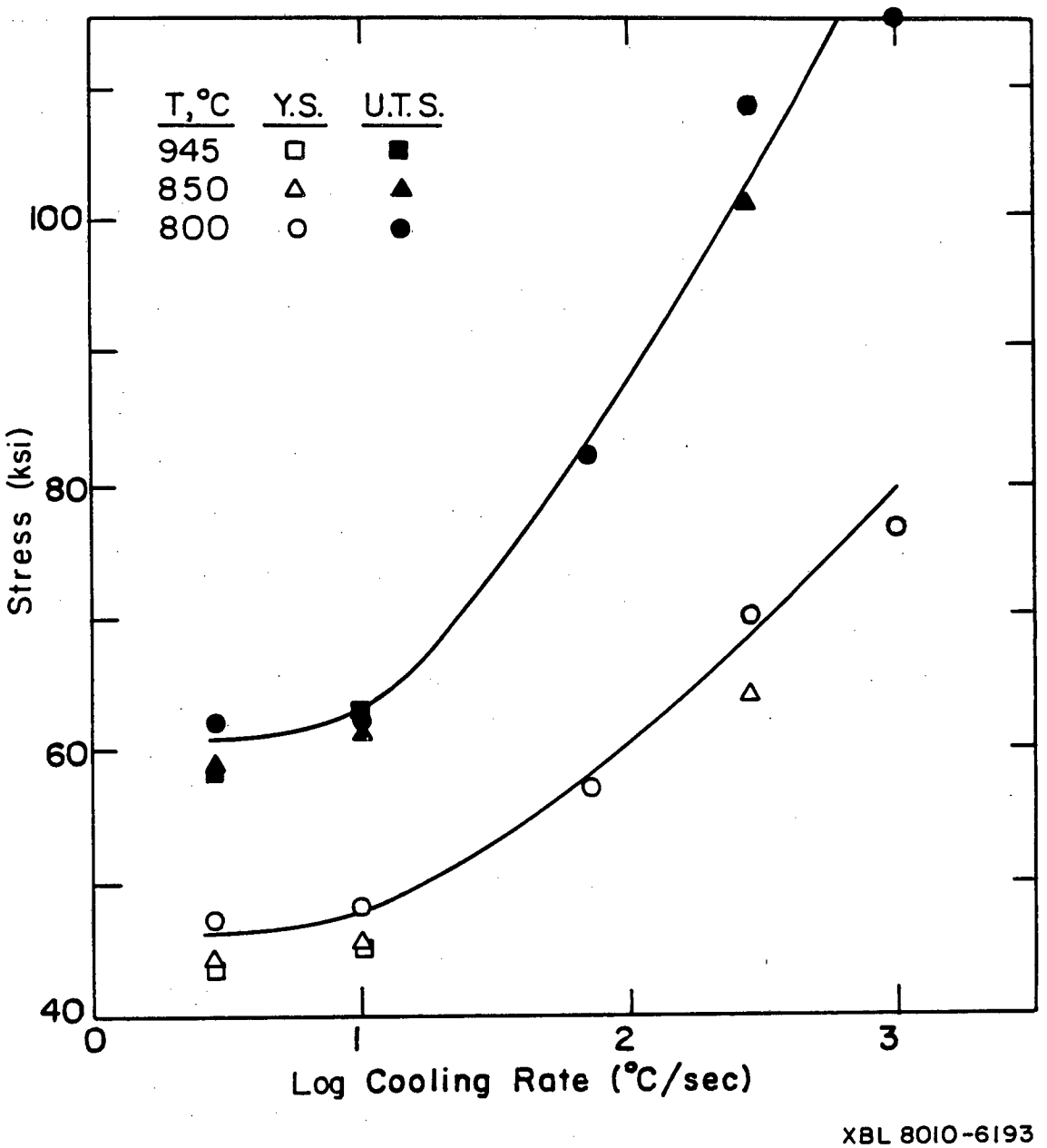
T,°C
Y.S.
U.T.S.
945
850
800
100
80
60
40
Stress (ksi)
0
1
2
3
Log Cooling Rate (°C/sec)
XBL 8010-6193

Fig. 8

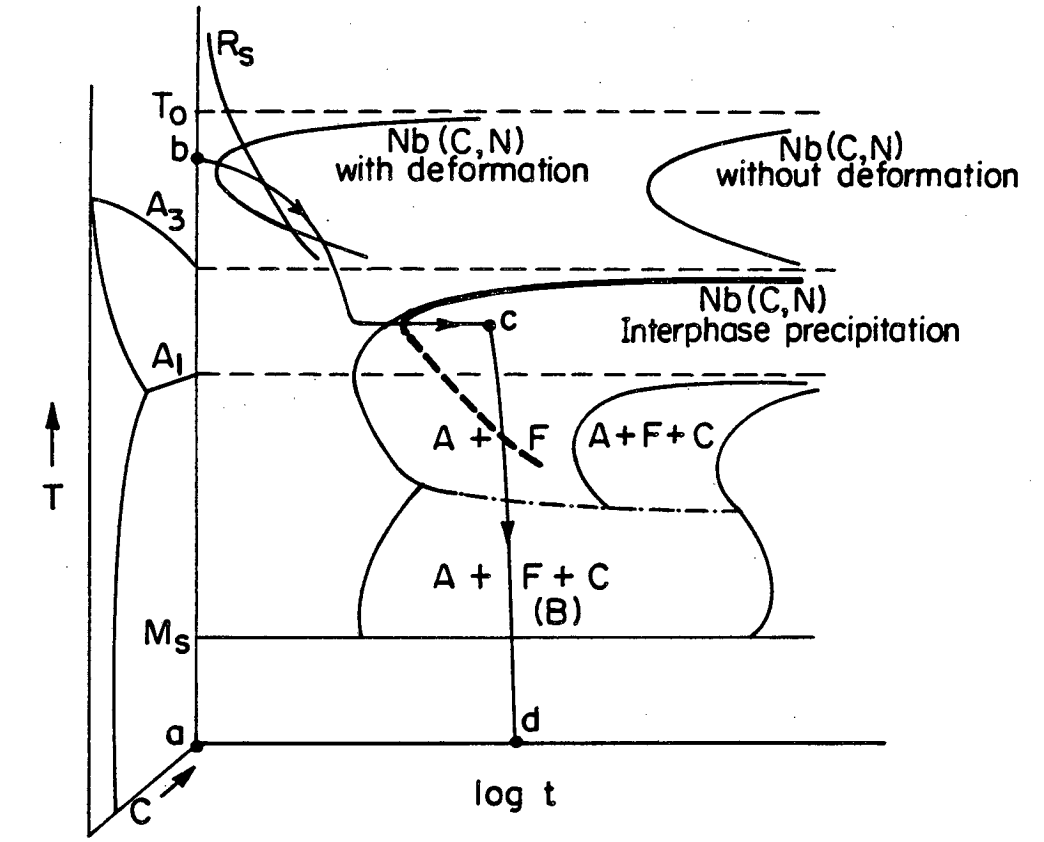

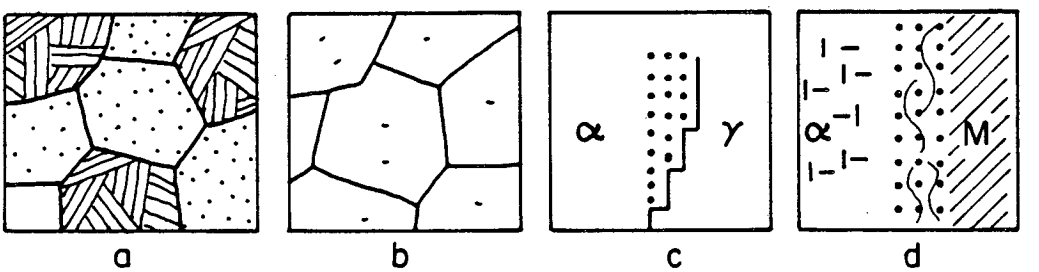

T_O = Precipitate Solubility Temperature

M_S = Martensite Start Temperature

A = Austenite, F = Ferrite, C = Carbide

R_S = Recrystallization Start Curve

XBL 819-6637

Fig. 9

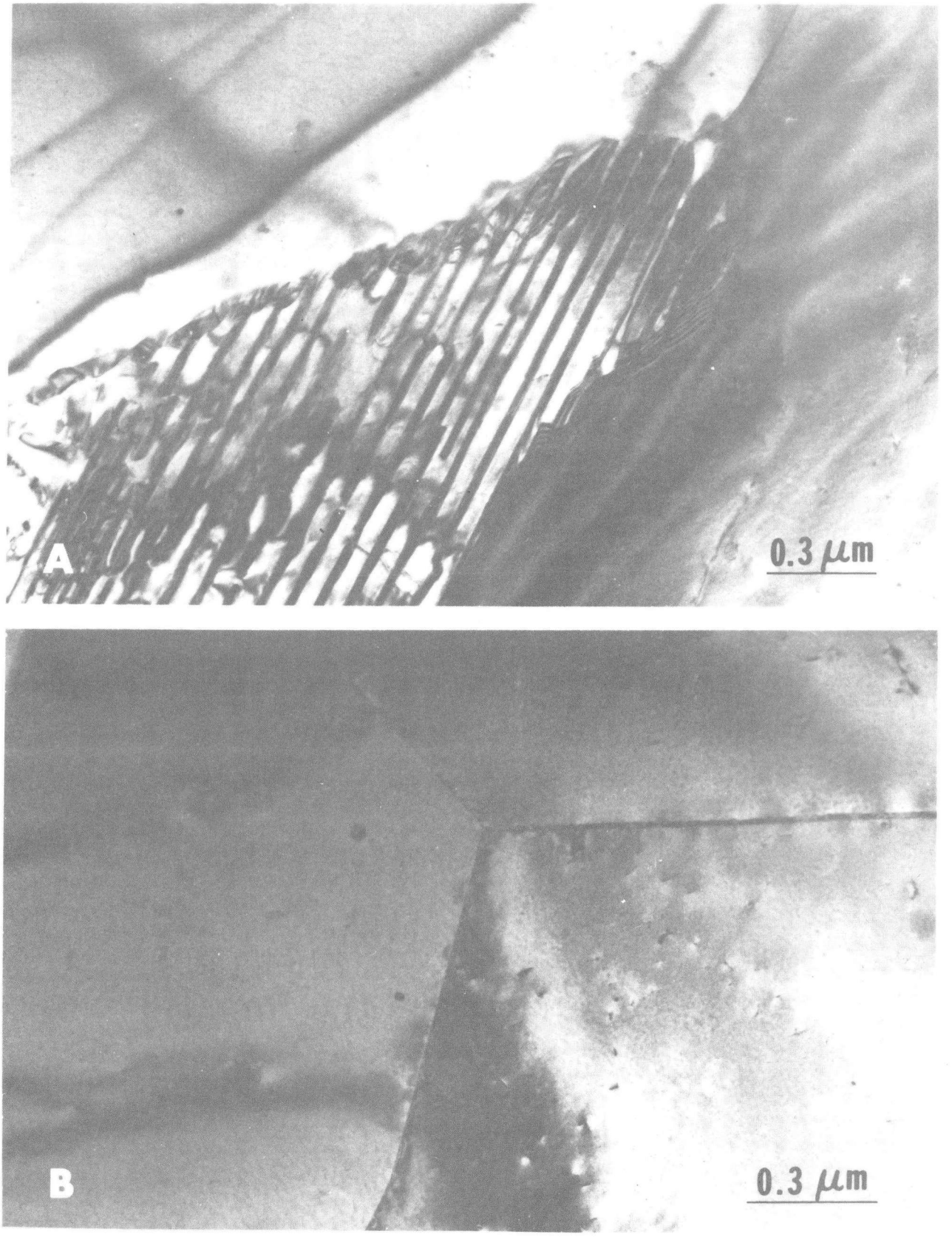

XBB 819-8863

Fig. 2

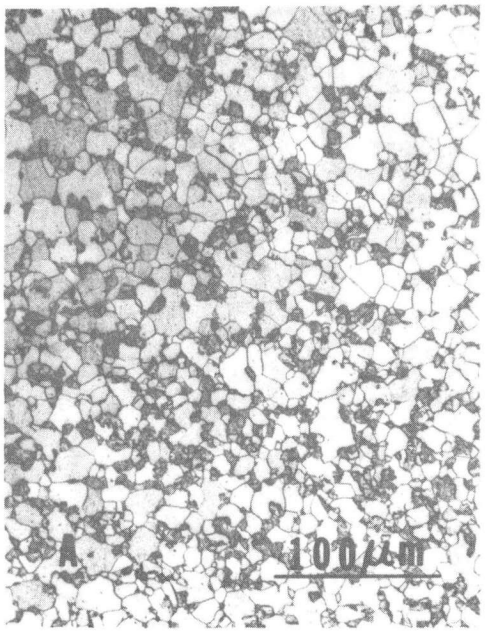

Process I
Intercritical Annealing

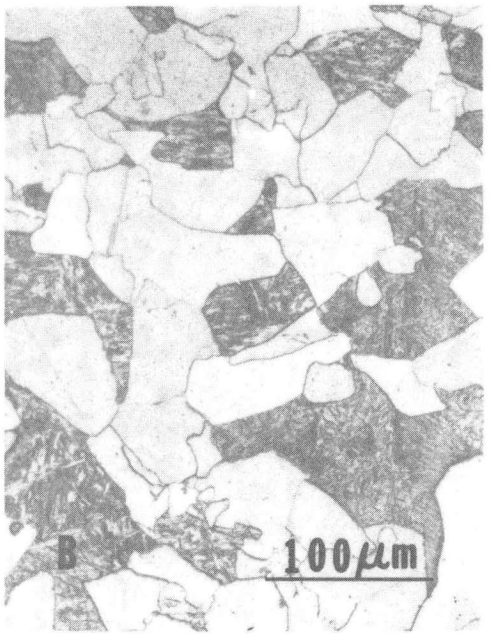

Process II
Intercritical Annealing

Process III
Intercritical Annealing

XBB 800-14028

Fig. 3

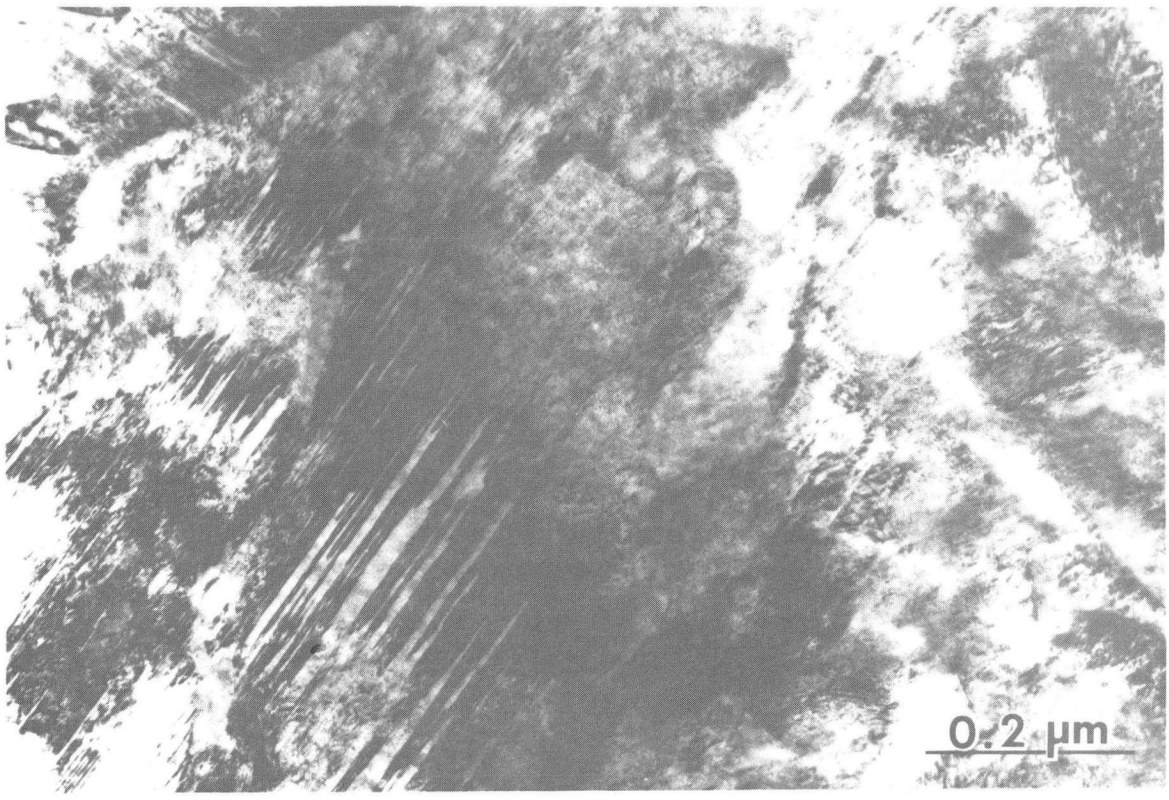

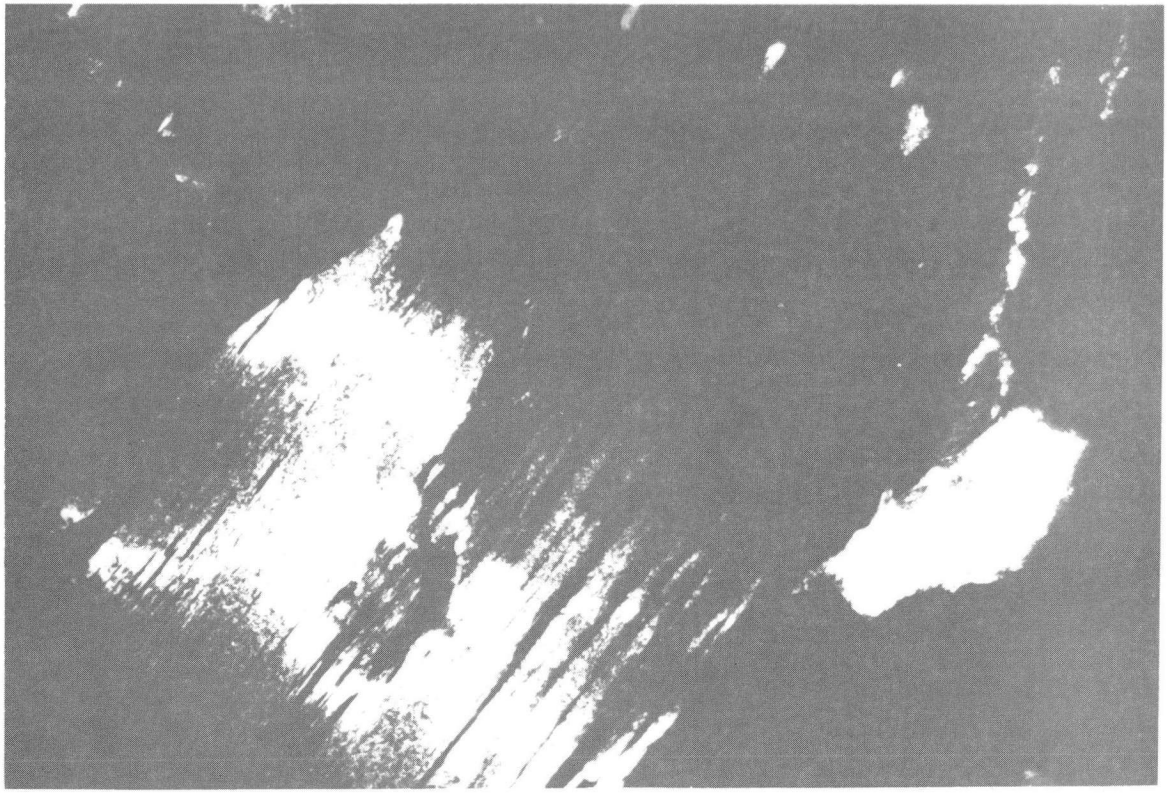

XBB 800-11960

Fig. 4

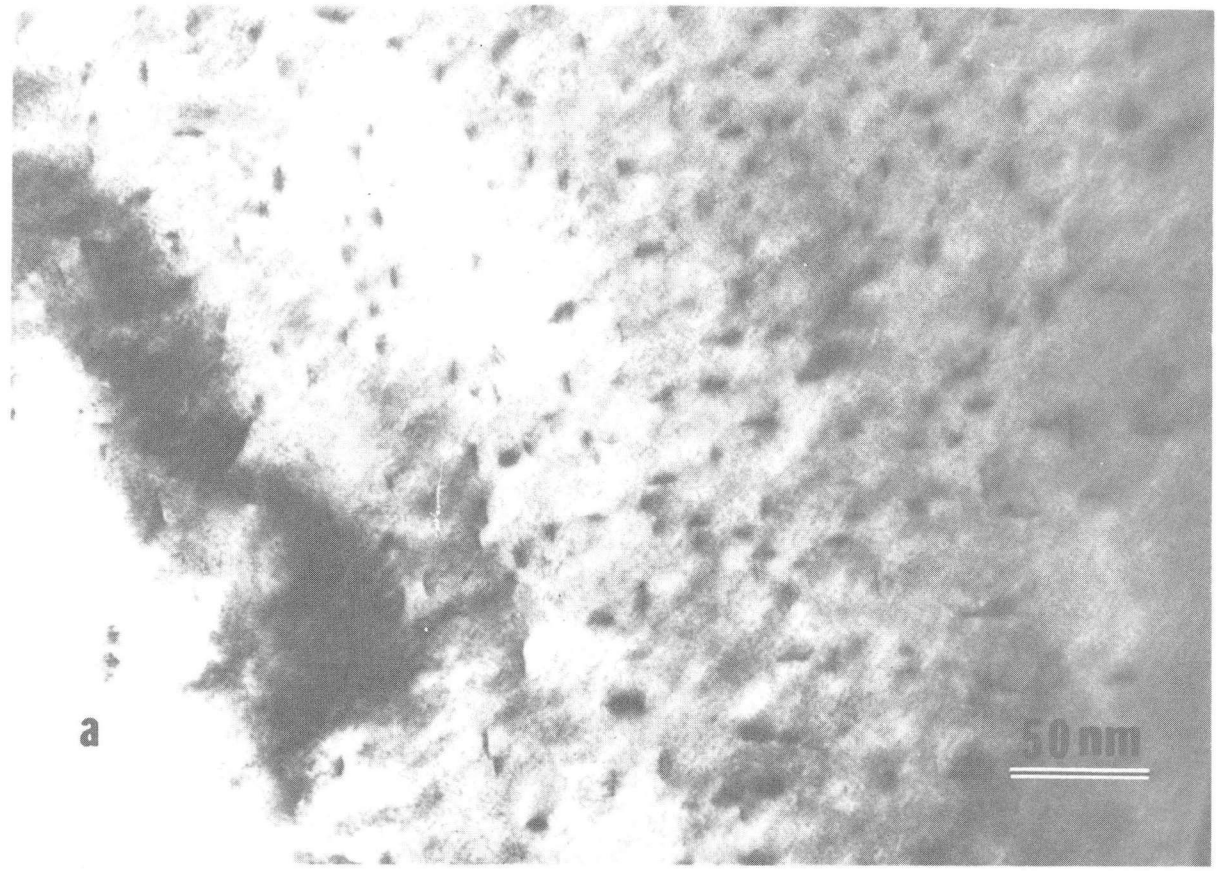

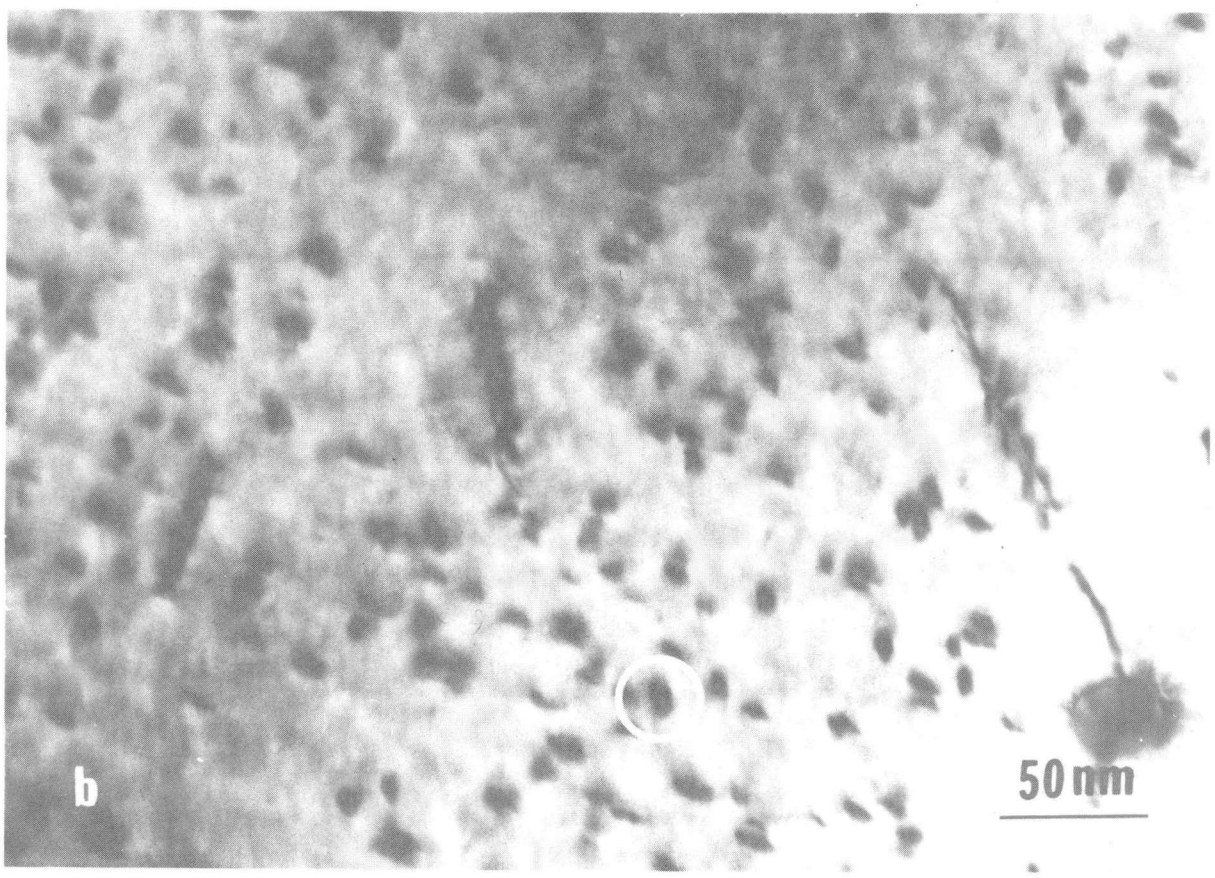

XBB 819-8862

Fig. 5

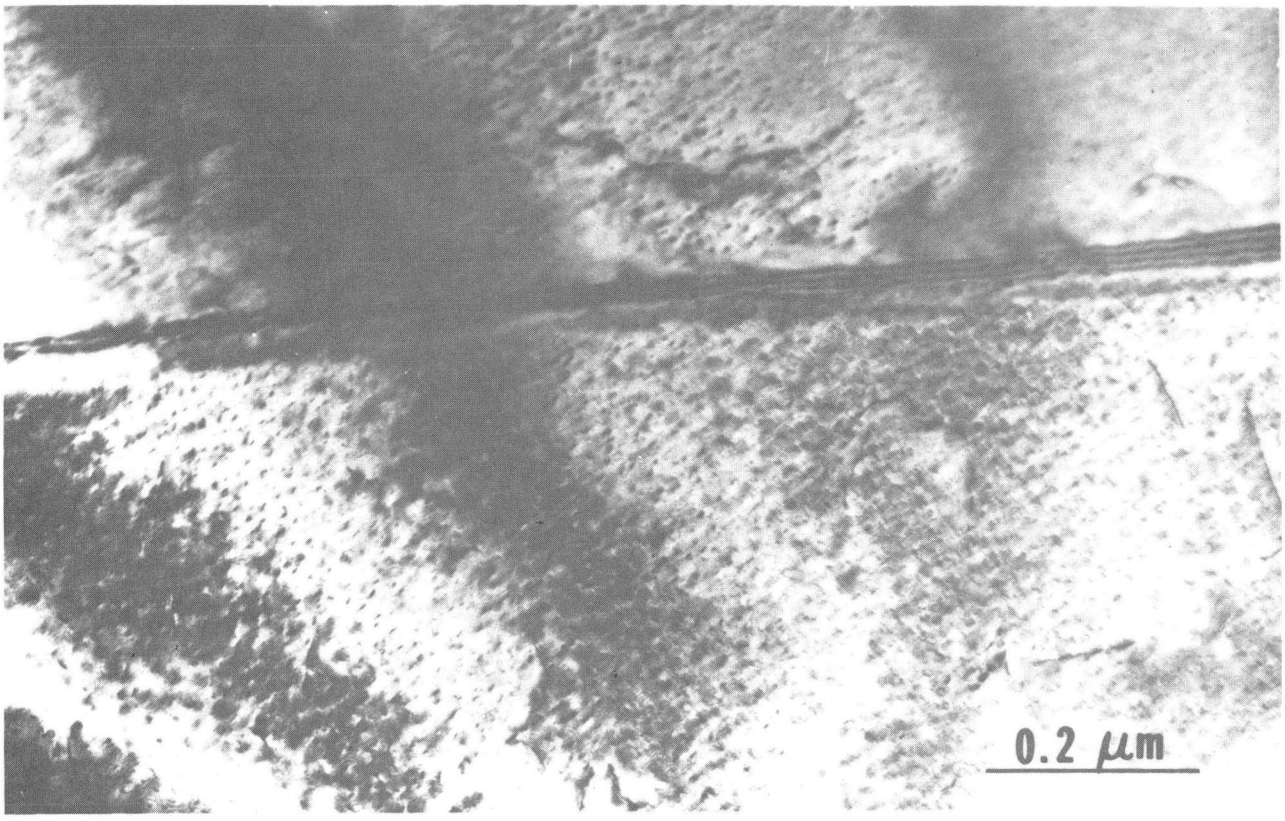

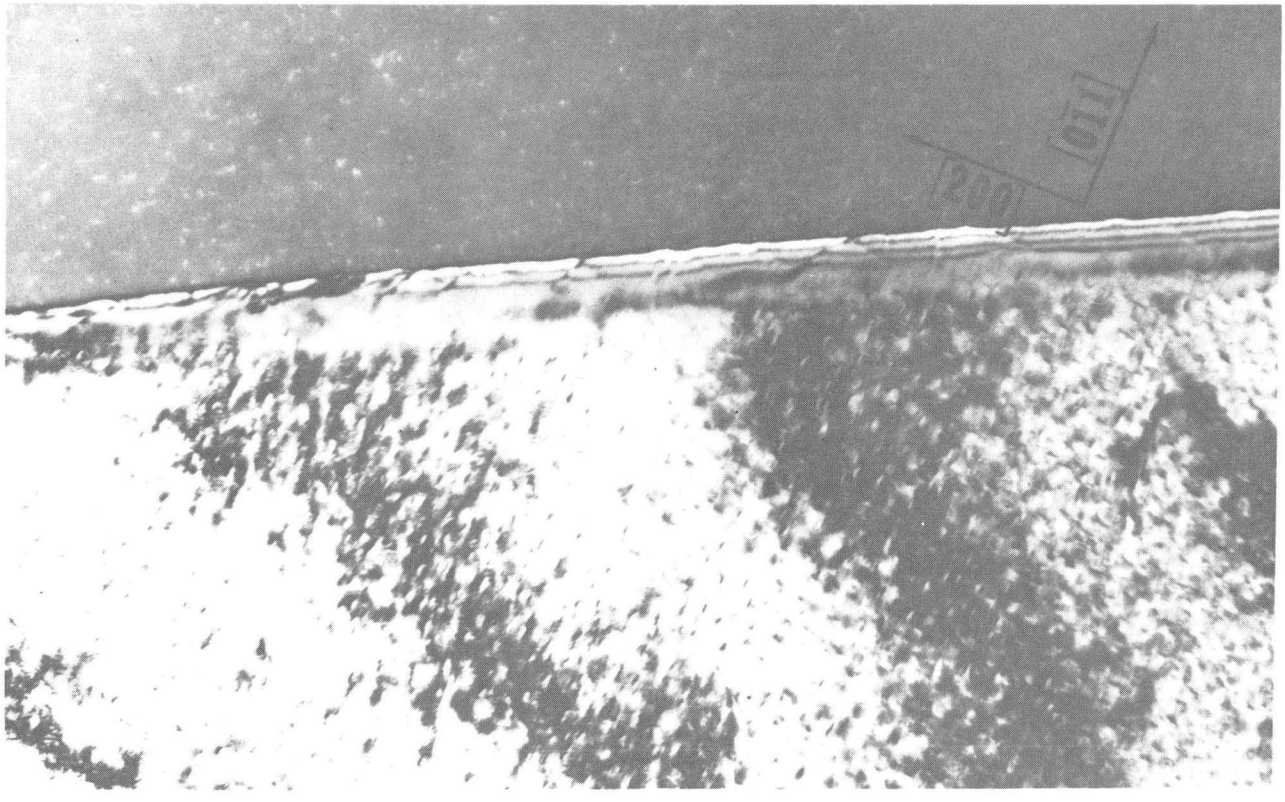

XBB 800-11952

Fig. 6

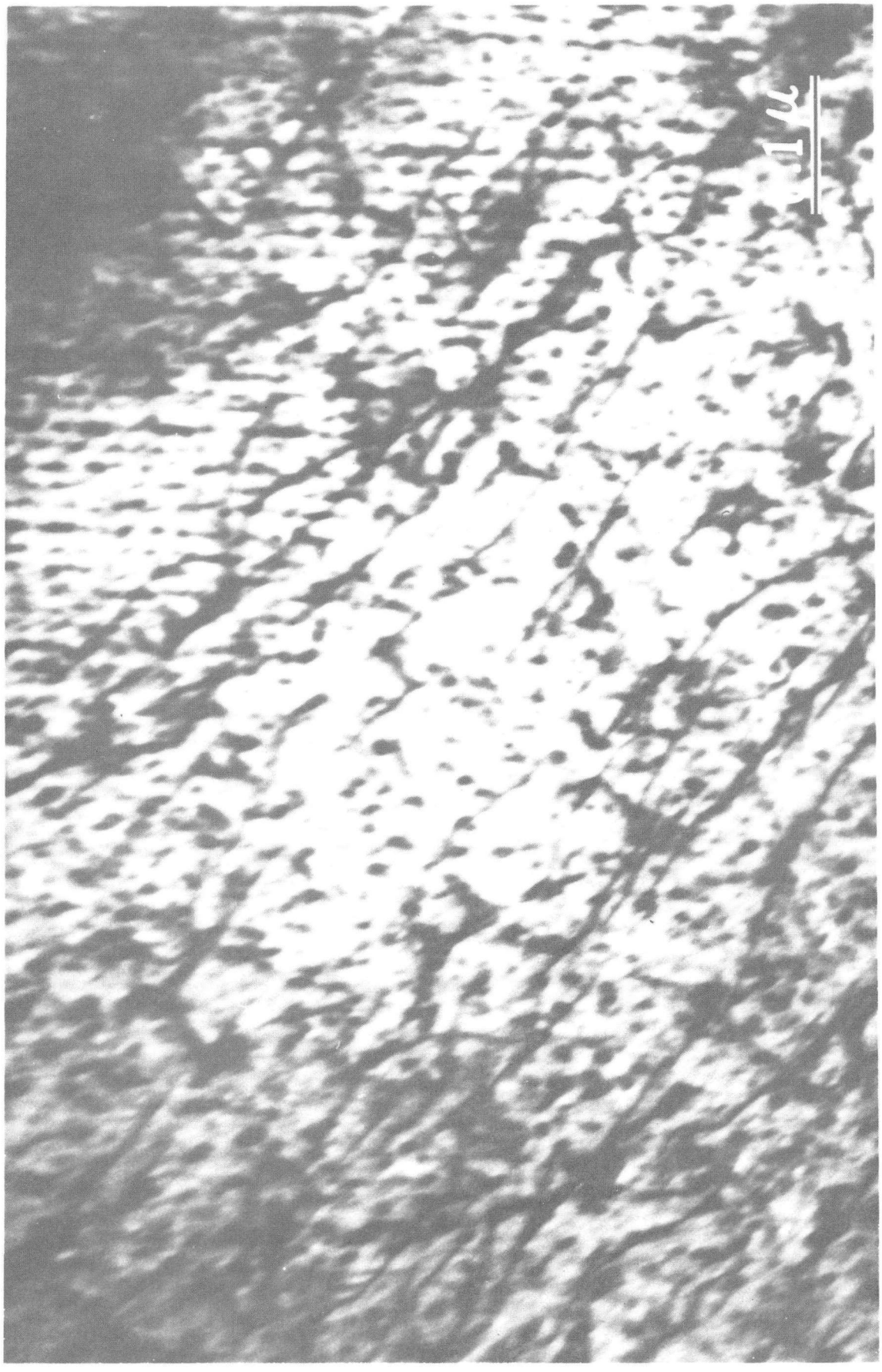

XBB 819-8361

Fig. 7

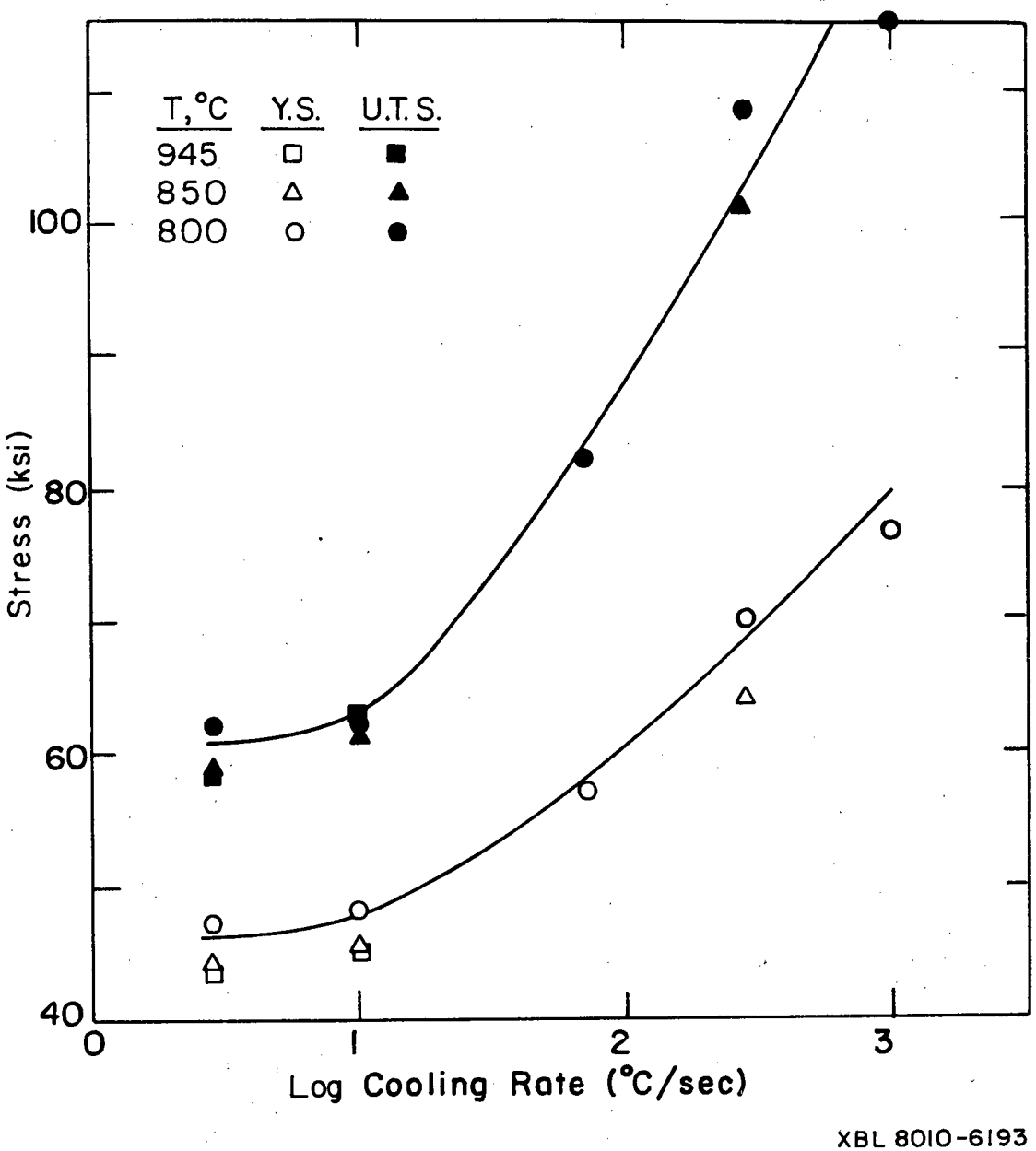
T,°C
Y.S.
U.T.S.
945
850
800
100
80
60
40
Stress (ksi)
0
1
2
3
Log Cooling Rate (°C/sec)
XBL 8010-6193

Fig. 8

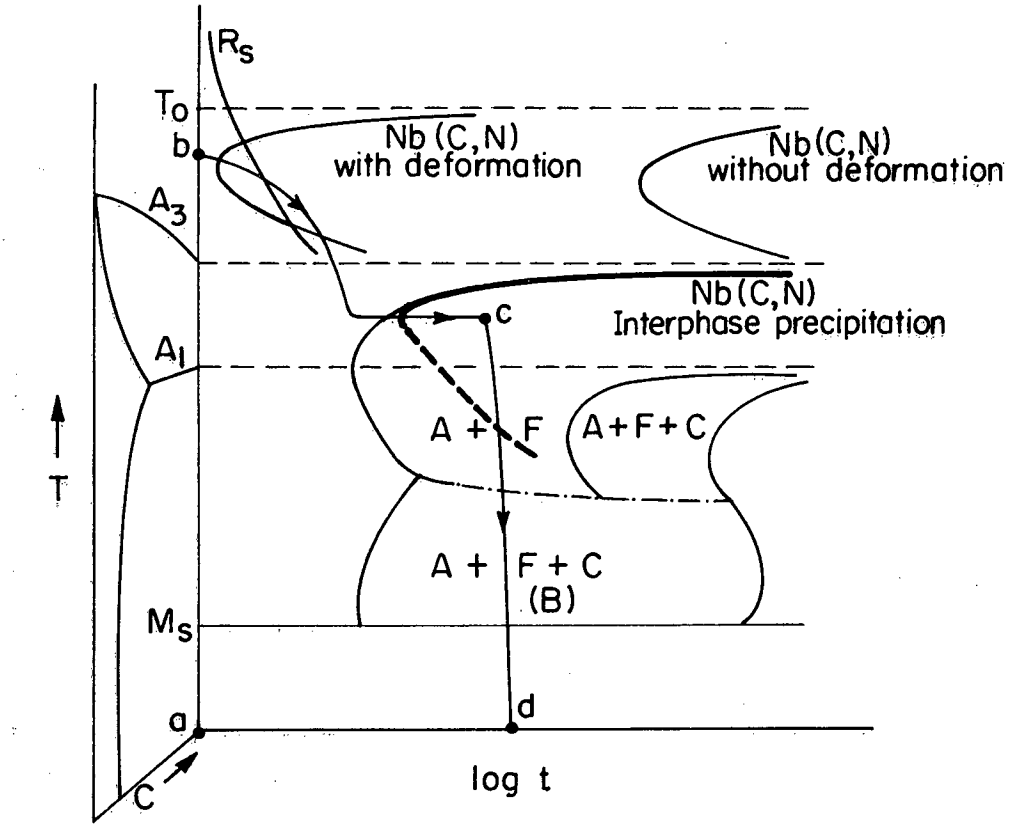

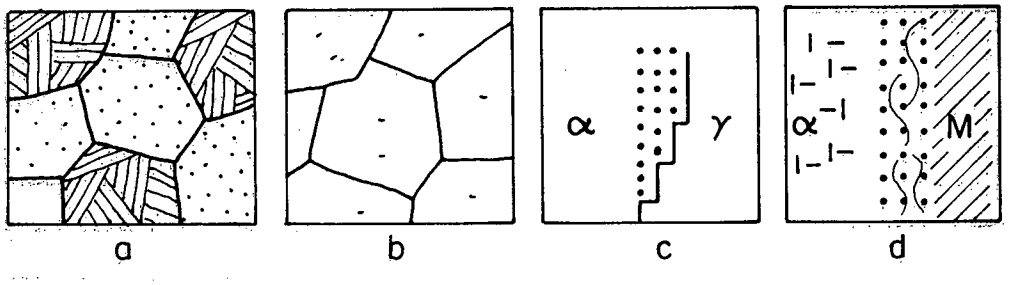

T_o = Precipitate Solubility Temperature

M_s = Martensite Start Temperature

A = Austenite, F = Ferrite, C = Carbide

R_s = Recrystallization Start Curve

XBL 819-6637

Fig. 9

TECHNICAL INFORMATION DEPARTMENT
LAWRENCE BERKELEY LABORATORY
UNIVERSITY OF CALIFORNIA
BERKELEY, CALIFORNIA 94720